Cooling Effects in Multiscan Laser Forming

Jin Cheng and Y. Lawrence Yao
Department of Mechanical Engineering, Columbia University
New York, NY 10027

Abstract

For laser forming of sheet metal to become a practical production or rapid prototyping tool, multiscan, that is, to use a laser to scan the workpiece repeatedly is necessary in order to achieve the required magnitude of deformation. Between consecutive scans, substantial waiting time is normally necessary for the workpiece to cool down in order for a steep temperature gradient to be reestablished in the next scan. In this paper, cooling effects under various conditions including different laser power, scanning speed, nozzle offset and cooling air pressure are investigated. Cooling effects on microstructure change and other mechanical properties including strength, ductility and hardness are also examined. The investigation on multiscan laser forming shows forced cooling has the potential to significantly reduce the total forming time while having no undesirable effects on microstructure change and other mechanical behavior. The established numerical model for laser forming with forced cooling provides greater insights into the cooling effects on deformation mechanism, helps predict such effects on final dimensional accuracy and mechanical properties, and can be extended to optimize the multi-scan laser forming process.

1. Introduction

Laser forming involves laser-induced thermal distortion to shape sheet metal without hard tooling or external forces. Compared with the traditional metal forming technologies, laser forming has many advantages. The cost of the forming process can be reduced because no tools or external forces are involved in the process. This is especially useful for small batch and high variety of sheet metal components. With the high flexibility in the laser beam's delivering and power regulating systems, it is easy to incorporate laser forming into an automatic flexible manufacturing system. Laser forming uses localized heating to induce controlled deformation and therefore has the advantage of energy efficiency.

Despite these advantages, progress needs to be made for laser forming to become a practical processing technology. For instance, multiscan is necessary for large deformation and complex 3-D laser forming. The waiting time between scans can be significant if there is no forced cooling. This is because, if the workpiece is not cooled sufficiently close to room temperature after a scan, the temperature gradient required in laser forming may not be readily reestablished in the next scan. Furthermore, the aggregated heat may result in surface melting.

Sprenger, et al. (1994) extensively investigated multi-scan laser forming. They showed that decrease of absorption coefficient, increase of the sheet thickness, and work hardening of the material affect the decrease of bending angle with increasing number of irradiations. However, they did not address the cooling issue. Odumodu and Das (1996) suggested to use forced cooling in multi-scan laser forming but did not investigate its effects. Hennige and Geiger (1999) have experimentally investigated cooling in multi-scan laser forming of aluminum sheets. They suggested high-pressure air-cooling, passive and active water-cooling and showed that, compared with air-cooling, active water-cooling reduces the entire processing time by increasing the bend angle per scan. They also showed that both air-cooling and water-cooling have no detrimental effects on the microstructure of the formed parts. Although it was shown that active water-cooling is more efficient, it is inconvenient in industrial settings. Moreover, it complicates the process by introducing laser-liquid-solid interactions and requires an additional liquid container and circulation system.

This paper presents experimental and numerical investigations aimed at gaining better understanding of cooling effects in single and multi-scan laser forming. Experimentally validated numerical results provide greater insights into cooling effects on deformation characteristics, temperature profile, stress distribution and process efficiency. Cooling effects on microstructure and other mechanical properties are also examined. These results help predict such effects on final dimensional accuracy and mechanical properties.

2. Forming process with forced cooling

The following general assumptions have been made. The workpiece material is isotropic, has constant density, and is opaque, i.e., the laser beam does not penetrate appreciably into the solid. The power density distribution of the laser beam follows a Gaussian function. The laser operates in continuous wave (CW) mode. Material properties such as the modulus of elas-

ticity, heat transfer properties, thermal conductivity, specific heat, and flow stress are temperature dependent (Grigoriev and Meilikhov, 1997; Lampman and Zorc, 1990). The rate of deformation is the total strain rate that is the sum of the elastic, viscous, and plastic strain rate. The strain-hardening coefficient is also temperature dependent. Energy dissipated through plastic deformation is negligible compared with the intensive laser energy involved. No melting is involved in the forming process. It is assumed that the residual stress of the workpiece before laser forming is negligible. Finally, no external forces are applied to the solid. Stresses occur only due to thermal expansion or contraction.

Heat transfer:

The transient conduction for a solid workpiece of dimension *L by W by d* (Fig. 1), radiated by a laser beam can be expressed in terms of temperature as:

$$\rho c_p \frac{\partial T}{\partial t} = \nabla \cdot (k \nabla T) \qquad (1)$$

subject to the boundary conditions: y=0: $T \to T_\infty$; y=W: $T \to T_\infty$; z=0: $\alpha_{abs} F \cdot \hat{n} = -\hat{n} \cdot (k \nabla T)$, $Q_{conv} = h_{z=0}(T - T_\infty)$, and $Q_{rad} = \varepsilon\sigma(T^4 - T_\infty{}^4)$; z=d: $Q_{conv} = h_{z=H}(T - T_\infty)$, and appropriate initial conditions such as t=0: $T(x, y, z, 0) = T_\infty$ where ρ, c_p, k *and* α_{abs} are the density, specific heat, thermal conductivity, and the material's absorbency, respectively. The symbols, *x, y,* and *z* are the Cartesian coordinates (Fig. 1); $\hat{n}$ is the unit vector normal to the surface pointing to the solid*;* and Q_{rad} and Q_{conv} are the heat flux due to the convection and radiation, respectively. The heat transfer coefficient due to the impinging jet on the top and bottom surface of the solid are $h_{z=0}$ and $h_{z=d}$ respectively; ε and σ are the emissivity and Stefan-Boltzmann constant, respectively. T is the temperature of the plate and T_∞ is the ambient temperature.

The heat flux due to the Gaussian distributed laser power is expressed as:

$$F = Q_{\max} \exp(-R_k R^2)$$
$$Q_{\max} = P_{laser} R_k / \pi \qquad (2)$$

where Q_{max} is the heat flux intensity of the laser beam, R is the distance to the laser beam center, R_k is the concentration coefficient, and P_{laser} is the laser power.

Heat convection due to the cooling jet(s):

Simple converging nozzles with circular cross-section are assumed. The following equations correlate the integral mean values (Martin, 1977)

$$\left(\frac{\overline{Nu}}{\Pr^{0.42}}\right)_{SRN} = \frac{D}{R} \frac{1 - 1.1D/r}{1 + 0.1(H/D - 6)D/r} F(\mathrm{Re})$$
$$\text{for } 2.5 \le r/D \le 7.5$$

$$\left(\frac{\overline{Nu}}{\Pr^{0.42}}\right)_{SRN} = F_1(\mathrm{Re}, r/D) k(H/D, r/D)$$
$$\text{for } 0 \le r/D \le 2.5 \qquad (3)$$

where *Re*, *Nu*, and *Pr* are Reynolds, Nusselt, and Prandtl number, respectively, H is offset - the vertical distance of the nozzle to the sheet surface, D is the diameter of the nozzle, and r the radial distance from the nozzle center. The above equations are valid for $2{,}000 \le Re \le 4{,}000{,}000$ and $2 \le H/D \le 12$. The function *F(Re)* can be represented by the following smooth curve expression

$$F(\mathrm{Re}) = 2\,\mathrm{Re}^{1/2}\left(1 + \frac{\mathrm{Re}^{0.55}}{200}\right)^{0.5} \qquad (4)$$

F_1 *(Re, r/D)* and *k (H/D, r/D)* are represented graphically. For the experiments reported in this paper, the Reynolds number ranges from 1×10^6 to 4×10^6 around the stagnation point.

The angle of incidence of the jet relative to the impinged surface relocates the point of maximum heat transfer and reduces the heat transfer rate, but the average heat transfer coefficient remains essentially unchanged. For the present study, the angle of incidence remained less than 10 degrees away from the vertical position and therefore its effect is neglected.

Thermal stress:

Assume the faces (z=0 and d) of the workpiece plate are free of traction, that is, $\underline{\underline{\sigma}} \cdot \hat{n} = 0$ and the edges (x=0, y=0, x=L, y=W) have no traction and no clamped boundary conditions (Fig. 1). The plate is assumed to be initially free of stress. Since the initial stress distribution is prescribed, it may be integrated forward in time to obtain the unique stress distribution for all times. Under the conditions given by the heat transfer portion, the stress and strain distribution is solved using the following sets of equations:

Since there are no external forces, body forces and acceleration components, the entire stress distribution of the part obeys $\nabla \cdot \sigma = 0$, or

$$\frac{\partial \sigma_{ij}}{\partial x_j} = 0 \qquad (5)$$

The relationship between the states of stress in the plate at time *t*, the state of strain in the plate at time *t* and the rate of change of the prescribed temperature distribution at that time follows. The total strain rate $\dot{\varepsilon}_{ij}$ is composed of the mean strain rate $\dot{\varepsilon}_{kk}$ and the deviatoric strain rate $\dot{e}_{ij}$. The mean strain rate is given by

$$\dot{\varepsilon}_{kk} = \frac{1 - 2\nu}{3E} \dot{\sigma}_{kk} + \alpha \dot{T} \qquad (6)$$

where E is Young's modulus, v is the Poisson's ratio, σ_{kk} is the mean stress, and α is the thermal expansion coefficient. For laser forming processes at high stress and temperature levels the viscoelastic effect may both be significant. Thus, the deviatoric strain e_{ij}, which is composed of an elastic portion e_{ij}^{E}, a viscoelastic portion e_{ij}^{v}, and a plastic portion e_{ij}^{P}, can be written as

$$\dot{e}_{ij} = \dot{e}_{ij}^{E} + \dot{e}_{ij}^{V} + \dot{e}_{ij}^{P} \qquad (7)$$

where

$$\dot{e}_{ij}^{E} = \frac{1}{2\mu}\dot{s}_{ij} \text{ and } \dot{e}_{ij}^{v} = \frac{1}{2\eta}s_{ij} \qquad (8)$$

where μ is the shear modulus, η is the viscosity constant, and s_{ij} the deviatoric stress component. e_{ij}^{P} is assumed to be governed by flow rules associated with perfectly plastic behavior and the Von mises yield criterion, that is,

$$e_{ij}^{P} = 0 \text{ if } \frac{1}{2}s_{ij} < k^2(T), \text{ or if } \frac{1}{2}s_{ij} = k^2(T) \text{ and } s_{ij}\dot{s}_{ij} - 2kk'\dot{T} \le 0$$

$$e_{ij}^{P} = \lambda s_{ij} \text{ if } \frac{1}{2}s_{ij} = k^2(T) \text{ and } s_{ij}\dot{s}_{ij} - 2kk'\dot{T} \ge 0 \qquad (9)$$

where $\dot{s}_{ij}^{v} = 2\mu(\dot{e}_{ij} - \dot{e}_{ij}^{\,v})$. s_{ij}^{v} is computed as though no plastic flow has occurred, although account is taken of he viscous flow. *k(T)* is the Von mises yield stress as a function of temperature. A function *g(x,t)* is introduced which is zero in the plastic state and unity elsewhere, that is,

$$g(x,t)=1 \text{ if } \frac{1}{2}s_{ij} < k^2(T), \text{ or if } \frac{1}{2}s_{ij} = k^2(T) \text{ and } s_{ij}\dot{s}_{ij} - 2kk'\dot{T} \le 0$$

$$g(x,t)=0 \text{ if } \frac{1}{2}s_{ij} = k^2(T) \text{ and } s_{ij}\dot{s}_{ij} - 2kk'\dot{T} \ge 0 \qquad (10)$$

Therefore, the combined stress-strain relations from equations (7) to (10) can be written as (Boley and Weiner, 1997)

$$\dot{\varepsilon}_{ij} = \frac{1+v}{E}\dot{\sigma}_{ij} - \delta_{ij}\frac{v}{E}\dot{\sigma}_{KK} + \left(\frac{1}{2\eta} + 2(1-g)\lambda\right)\left(\sigma_{ij} - \delta_{ij}\frac{\sigma_{kk}}{3}\right) + \delta_{ij}\alpha\dot{T} \qquad (11)$$

Numerical simulation:

Since the heat transfer and viscoelastic/plastic deformation are symmetric about the vertical plane containing the scanning path, only half of the plate is modeled in the numerical simulation. The symmetric plane is assumed to be adiabatic. The same mesh model is used for the heat transfer analysis and structural analysis. Two adjacent points in the middle of the symmetric plane are assumed to be fixed in order to remove the rigid body motion. All other points within the symmetric plane are assumed to move only within the symmetric plane throughout the deformation process. A commercial code, ABAQUS, is used to solve the heat transfer and structural problem. In structural analysis, the twenty-node element has no shear locking, no hourglass effect, and is thus suitable for a bending-deformation-dominated process such as laser forming. On the other hand, the eight-node element suffers from "shear locking," and is therefore not suitable for such a process. In order to remain compatible with the structural analysis, a twenty-node element is used in heat transfer analysis.

3. Experiment

The straight-line laser forming with forced air cooling is schematically shown in Fig. 1. The scanning path is along the *x*-axis and the direction perpendicular to the scanning path and within the plate is defined as *y*-axis. Multiscan is performed over the same line. To avoid severe edging effect, multiscan is performed back and forth along *x*-axis. A simple converging nozzle with circular cross section was used. The angle of incidence of the impinging jet relative to the sheet surface, β, was kept close to 90 degrees to create higher convection heat transfer at the stagnation point.

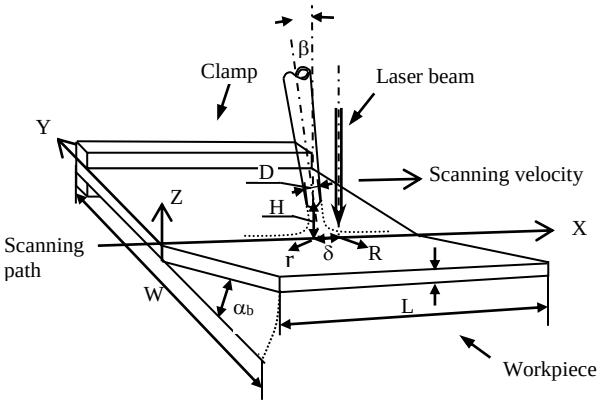

Fig.1 Laser forming system with cooling jets

The diameter of the nozzle, *D*, is 1.6mm and the stand-off distance, *H*, is 8mm. Most experiments were done with zero offset between the impinging jet stagnation point and the laser beam center although the effect of the offset distance δ was also investigated.

The material is low carbon steel, AISI 1010, and 80mm by 80mm by 0.89mm in size. To enhance laser absorption by the workpiece, graphite coating is applied to the surface exposed to the laser.

Most experiments use laser power of 400 or 800 W except one uses varying power from 400 to 800 W. Most experiments use scanning velocity of 25 or 50

mm/s except one uses velocity varying from 25 to 80 mm/s. Most experiments use air pressure of 80 psi except one uses pressure varying from 0 to 80 psi. Most experiments use a laser beam size of 4 mm except one uses 8 mm to induce the buckling mechanism (BM). Most experiments use zero offset except one uses offset δ varying from 0 to 18 mm. Most experiments use bottom surface cooling only except one uses top surface cooling and both bottom and top surface cooling. The exact experimental conditions are noted in the Figures and their legends. All the experiment conditions were repeated three times. Standard deviations were shown in terms of error bars in subsequent figures.

The laser system used is a PRC-1500 CO_2 laser, which has a maximum output power of 1,500 W. A coordinate measuring machine (CMM) is used to measure the bending angle of the formed parts. To calculate the Reynolds number of the air at the nozzle exit that is applied in the numerical simulation, a velocimeter is used to measure the velocity of the air at the nozzle exit. A scanning electron microscopy is used to investigate the microstructure of the material after laser forming. Tensile test samples are machined by CNC along the scanning path and tensile tests are conducted on a MTS. A Rockwell hardness tester is used to measure the hardness of the material after laser forming.

4. Results and discussion

4.1 Simulation validation and cooling effect on deformation

Figs. 2 (a) and (b) compare simulation and experimental results under a wide range of conditions and reasonable agreements are seen. Fig. 2 (a) shows the variation of the bending angle vs. scanning speed with and without cooling. As seen, the bending angle with cooling could be smaller or larger than that without cooling at a laser power of 400 W, while there is no appreciable difference between the two at 800 W. To help explain the phenomenon, peak temperature reached at the workpiece top and bottom surfaces as well as corresponding flow stress at these locations are plotted in Fig. 3 for P=400 W. Temperature, work hardening and strain rate effects were considered in determining the flow stress.

At the lower power of 400 W and lower velocity of 25 mm/s (Figs 2(a) and 3), the bending angle with cooling is lower than that without cooling by the greatest margin. Although the bottom-only cooling lowers the bottom temperature significantly (from about 850 K to 700 K) and therefore increases the temperature gradient between the top and bottom surface, which seems to favor more deformation, the cooling at the same time increases the flow stress at the bottom surface quite significantly (from about 120 to 170 MPa). The net result is a decreased bending angle.

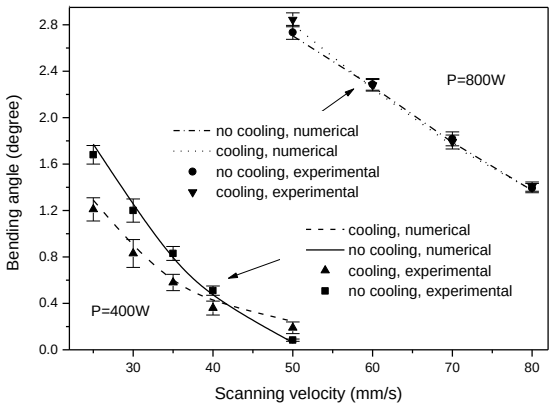

(a)

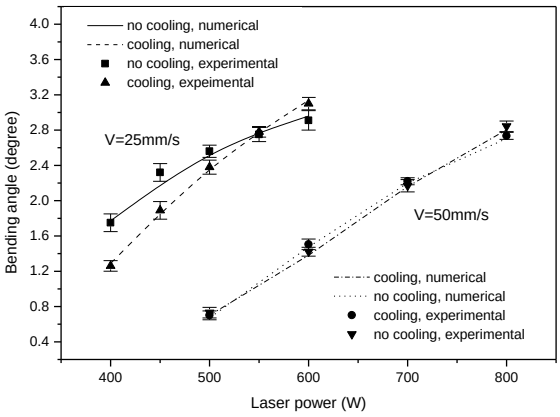

(b)

Fig.2 (a) Numerical and experimental bend angle vs. scanning velocity (b) Numerical and experimental bend angle vs. laser power. (D_{beam}=4mm, P_{air}=80psi, δ =0, bottom cooling only).

At the same power but higher velocity of 50 mm/s, the net result is opposite. This is because heat dissipation at this condition is lower due to the shorter cooling time and the temperature drop at the sample's surfaces is not as great as with the lower scanning speed. As a result, the cooling effect on temperature gradient increase begins to outweigh the cooling effect on flow stress increase.

At the higher power level of 800W (Figs. 2 (a)), the observation that the cooling effect on bending angle is not significant can be similarly explained using the temperature and flow stress. The flow stress used in the model is actually the Von Mises yield stress of the material, which is a function of temperature, strain, and strain rate (Li and Yao, 2000).

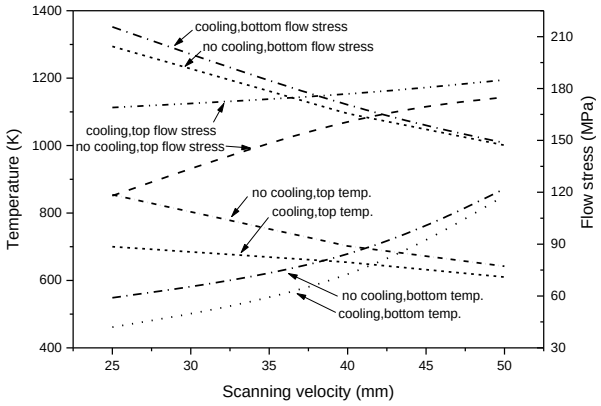

Fig. 3 Peak temperature and flow stress (P=400W, V=25mm/s, D_{beam}=4mm, P_{air}=80psi, δ =0, and bottom cooling only).

4.2 Effect of air pressure

Fig 4 (a) shows the relationship between the air-cooling pressure and the bending angle under two conditions. When the higher power of 800W and higher velocity of 50 mm/s is applied, the bending angle increases moderately with air-cooling pressure. This is because under this condition, the net heat input into workpiece is higher, the temperature drop due to the cooling is lower, and therefore the increase in flow stress is also lower. As a result, the temperature gradient increase between the top and bottom surfaces due to air-pressure increase is slightly more dominant. Fig. 4 (b) shows that the *y*-axis compressive plastic strain on the top surface only increases slightly when cooling (80 psi) is applied.

When a lower power of 400W and lower velocity of 25mm/s is applied, the bending angle decreases as the air-cooling pressure increases. This is because under the condition the net heat input is lower, the temperature drop due to the air-cooling is higher, and the increase in flow stress is higher. Although the temperature gradient between the top and bottom surfaces still increases with air-pressure, the cooling effect on the flow stress increase becomes dominant when the air pressure increases. This is evident in Fig 4 (b) where not only the *y*-axis compressive plastic strain but also the region of such plastic strain decrease as cooling (80 psi) is applied due to increased flow stress.

4.3 Effect of cooling nozzle offset

There exists a time delay between when the top surface reaches its peak temperature and when the bottom surface does due to heat conduction time. Therefore, if the impinging jet is placed coaxially with the laser beam, the cooling may not be the most efficient.

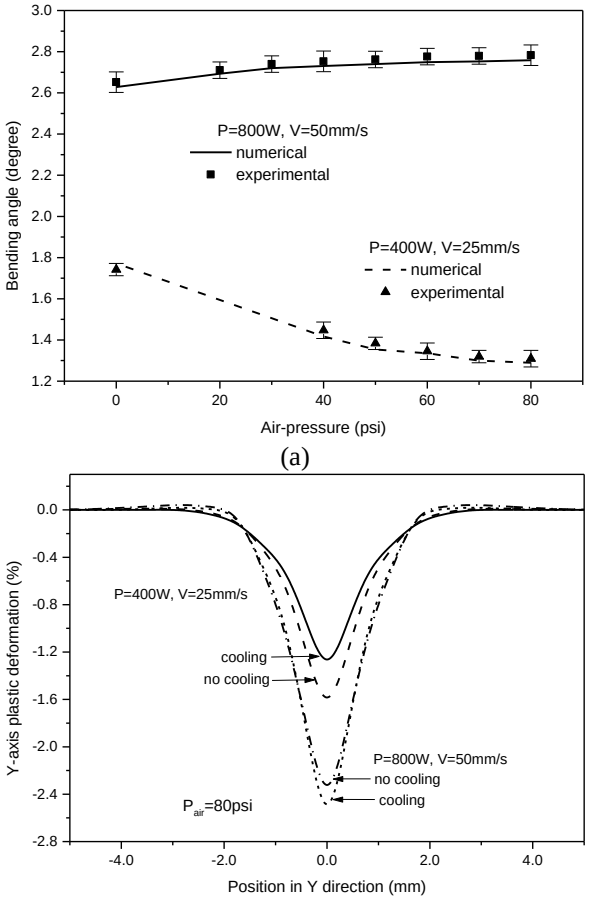

Fig. 4 (a) Bend angle vs. air pressure, and (b) The distribution of Y-axis plastic deformation along Y direction after laser forming with cooling and without cooling (D_{beam}=4mm, δ =0, bottom cooling only).

Fig 5. shows the effect of cooling nozzle offset δ (Fig. 1) on bending angle, where the cases of no cooling and cooling with zero offset are also shown. For the higher power of 800 W and higher velocity of 50 mm/s, the maximal bending angle is obtained when the offset is approximately 5 mm. For the lower power of 400 W and lower velocity of 25 mm/s, the minimal angle (under this condition, cooling causes the bending to decrease as seen in Fig. 2(a)) is obtained at offset about 2 mm. The difference between the two offset values can be easily explained because under the first condition the velocity is twice as large as that under the second condition. Therefore, there is a larger time delay between the top and bottom peak temperature under the first condition.

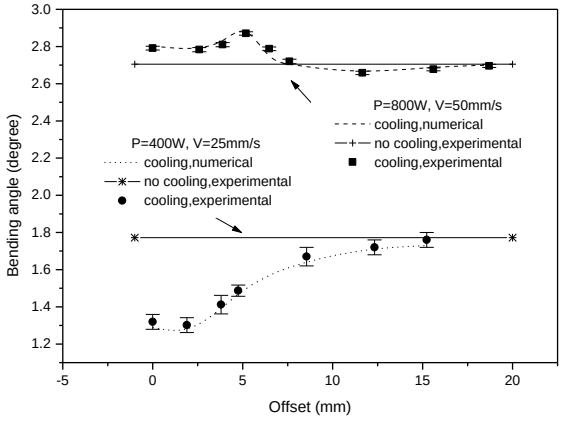

Fig. 5 Bend angle vs. offset δ
(D_{beam}=4mm, P_{air}=80psi, δ =0, bottom cooling only)

4.4 Microstructure

Grain structure:

Fig 6 (a) shows the SEM micrograph of the grain structure of AISI1010 steel before laser forming. Figs. 7 (a) and (b) show the SEM micrographs of the grain structure near the top surface after laser forming with and without cooling. It can be seen that the grain structure is refined after laser forming in both cases. The case with cooling (Fig. 7 (a)) exhibits a finer grain structure than the one without cooling (Fig. 7 (b)) obviously because of the higher cooling rate.

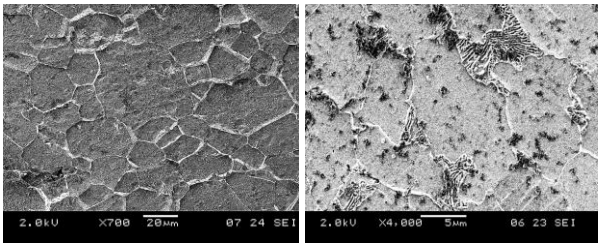

(a) (b)

Fig.6 SEM micrographs of the raw material (AISI1010 steel) (a) low magnification ($\times$ 700), and (b) high magnification($\times$ 4000) showing the phases (ferrite and pearlite).

During high temperature deformation, it is possible to have dynamic recovery and dynamic recrystalization. The ability for a material to do so depends on the stacking fault energy of the material (Courtney, 1990). Materials, such as aluminum alloys and steels, that have a high stacking fault energy do not dynamically recrystallize in a significant way. Therefore the grain refinement observed above is primarily due to static recovery and static recrystalization taking place after the material is plastically deformed and while it cools down to room temperature. The static recrystallization is affected by strain. The greater the strain the faster the recrystallization process, and the finer the grain size. Our results show that the grain size at higher laser power (P=800W) is finer than at lower laser power (P=400W) because the former undergoes larger plastic strain. The grains become even finer when cooling is applied as shown in Fig. 7 (a) obviously because of the higher cooling and nucleation rate.

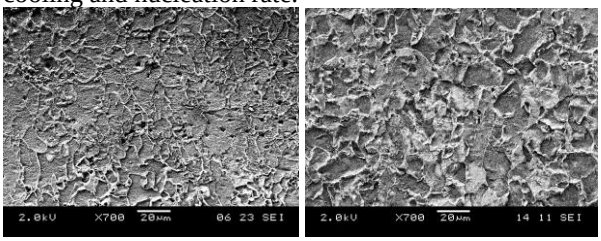

(a) (b)

Fig.7 SEM micrographs of grain structure near top surface after laser forming (a) with cooling and (b) without cooling. The grain structure with cooling is finer. (P=800W, V=50mm/s, D_{beam}=4mm, P_{air}=80psi, δ =0, bottom cooling only)

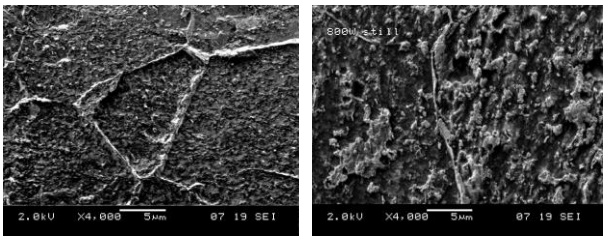

(a) with cooling (b) without cooling

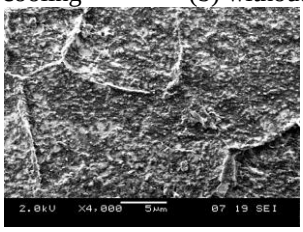

(c) 10 scans, with cooling

Fig. 8 SEM micrographs showing the microstructure of AISI1010 after laser forming under high magnification ($\times$ 4000). (a)&(b) after 1 scan, near top surface with cooling and without cooling, the bainite phase under cooling is finer and volume fraction is higher; (c) after 10 scans under cooling near top surface. (P=800W, V=50mm/s, D_{beam}=4mm, P_{air}=80psi, δ =0, bottom cooling only)

Phase transformation:

Fig. 6 (b) shows the SEM micrograph of the microstructure of the same as-received hypereutectoid steel at a higher magnification (x 4000), under which pearlite with ferrite background can be seen. Figs. 8 (a) and (b) show the SEM micrographs near the top surface after laser forming with and without cooling using the

same high magnification. During the transient heating to peak temperature, the material is heated to austenite region. After the material cools down, the final phases in the materials contain ferrite, bainite, and perhaps a small amount of pearlite. Figs. 8 (a) and (b) show that the microstructure near the top surface after laser forming with cooling contains a more refined bainite phase than that after laser forming without cooling. The bainite nucleates on the ferrite matrix and the nucleation rate is higher with the high cooling rate (Reed-Hill, 1973).

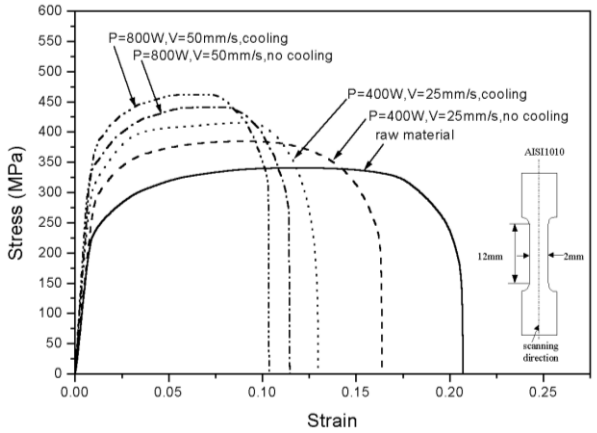

Fig. 9 Tensile stress-strain curves of workpiece before and after laser forming with and without cooling (D_{beam}=4mm, P_{air}=80psi, δ =0, bottom cooling only).

4.5 Mechanical properties

Fig 9. shows the tensile test results of laser formed specimen with and without cooling as compared with raw material. As shown in the lower right corner of Fig 9, the test length of the specimen is 12 mm and test width is 2 mm, with the laser-scanned region along its axis. It is seen that the yield strength of the material after laser forming is higher than that of the as-received material, the yield strength of the material under laser forming with cooling is higher than that under laser forming without cooling, and the yield strength of the material at higher laser power is higher than that at lower laser power. The reverse can be said about elongation before fracture. As discussed in Section 4.4, after laser forming the material's grain structure is refined, the material's phase change is from pearlite to refined bainite, and therefore the material is strengthened. The microstructure of materials under cooling shows a finer grain size and a finer bainite phase as compared with no cooling. Therefore, after laser forming the strength of the material with cooling is higher than without cooling. Comparing the conditions at higher and lower laser power, the former has more plastic deformation and a higher cooling rate, and therefore a finer grain size.

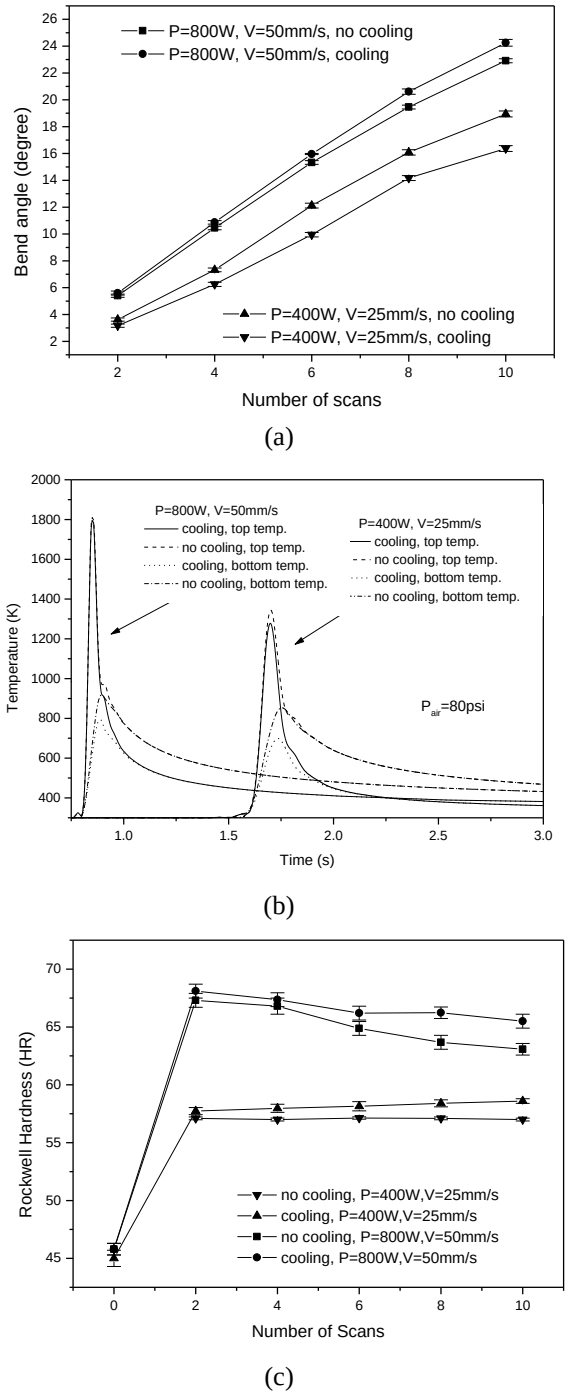

Fig. 10 (a) The development of bend angle vs. number of scans, (b) temperature history of a single scan with cooling and without cooling, and (c) Rockwell hardness vs. number of scans

4.6 Multiscan

Fig. 10 (a) shows the experimental results of the development of the bend angle as a function of number of scans. They show approximately linear patterns and indicate the work hardening effect is offset by the softening effect of the repeated laser scans. Although the

resultant bending angles with cooling and without cooling only differ moderately, the total times it takes for the ten scans to complete are vastly different. Without cooling, a substantial amount of time (in this case, about 150 second) has to be waited for the workpiece to cool down to near room temperature in order to be able to re-establish a steep temperature gradient during the scan immediately follows. With forced cooling, such a waiting period was reduced to about 10 seconds because the cooling rate with forced cooling is much higher as seen from the time history of temperature shown in Fig. 10 (b). As a result, the total forming time for the ten-pass processes reduced from about 23 minutes without cooling to less than two minutes with cooling. This shows cooling has the potential to greatly speed up multiscan operations, which are necessary if laser forming is to become a practical production tool. At the same time, it has been shown that cooling does not have major detrimental effects on efficiency, and mechanical properties.

Fig. 10 (c) shows the Rockwell hardness test results after multiscan under two different conditions. While the multiscan proceeds, strain hardening and recovery/recrystalization induced softening co-exist and compete with each other. At the higher power of 800W and higher velocity of 50mm/s, softening is more dominant due to higher temperature although the deformation is also larger. As a result, the hardness decreases somewhat when more scans are carried out. At the lower power of 400W and lower velocity of 25mm/s, the hardening and softening are about the same and as a result the hardness remains more or less constant while the number of scan increases.

Fig. 8 (c) shows the microstructure near the top surface after 10 passes of laser forming with cooling. For each pass in multi-scan laser forming, the material experiences the phase transformation to austenite, then to ferrite, bainite, and a small amount of pearlite. The phase structure after 10 passes shows no visible difference as that after one pass.

5. Conclusions

The cooling effect on forming efficiency varies with process conditions and the variation is discussed in terms of the competing effect on temperature and flow stress by the cooling. The forming efficiency is also experimentally and numerically investigated in terms of nozzle offset and cooling air pressure, and numerical results agree with experimental results.

Cooling significantly reduces the total forming time in multiscan laser forming by greatly reducing the need for waiting time between consecutive scans. Multiscan is necessary if laser forming is to become a practical production process. Cooling only moderately decreases material ductility even after multiscan since the repeated work hardening is offset by repeated softening. The softening is obtained through recovery and recrystallization accompanying each scan. Grain refinement and partial phase transformation to bainite are also observed.

Acknowledgment

Support for this project under a NSF grant (DMI-0000081) is gratefully acknowledged. Dr. Wayne Li's assistance in numerical study and experiments in particular is also greatly appreciated.

References

Boley, B. A., Weiner, J. H., 1997, Theory of Thermal Stresses, Dover Publications, Inc.

Courtney, T.H., 1990, Mechanical Behavior of Materials, Chapter 7, McGraw-Hill Series in Materials Science and Engineering

Hennige, T. D., Geiger, M., 1999, "Cooling effects in laser forming," Technical Paper -North American Manufacturing Research Institute of SME, pp.25-30

Li, W., Yao, Y.L., 2000, "Convex laser forming with high certainty," Trans. of the North American Manufacturing Research Institution of SME, pp.33-38

Magee, J., Watkins, K. G., Steen, W. M., 1998, "Advances in laser forming," Journal of Laser Application, Vol. 10, pp. 235-246

Martin, H., 1977, "Heat and mass transfer between impinging gas jets and solid surface," Advances in Heat Transfer, J.P Harnett and T.F. Irvine (Eds.), Vol. 13, Academic Press, New York, pp.1-60

Grigoriev, I. S. and Meilikhov, E. Z. (ed.), 1997, Handbook of Physical Quantities, CRC.

Lampman, S. R., and Zorc, T. B. (ed.), 1990, Metals Handbook, 10th edition, Vol.1, ASM International.

Odumodu, K.U., Das, S, 1996, "Forceless forming with laser," American Society of Mechanical Engineers, Materials Division (Publication) MD v 74, Nov. 17-22, pp.169-170

Reed-Hill, R.E., 1973, Physical Metallurgy Principles, Chapters 17 and 18, PWS-KENT series in Mechanical Engineering

Sprenger, A., Vollertsen, F., Steen, W. M., Watkins, K., 1994, "Influence of strain hardening on laser bending," Laser Assisted Net Shape Engineering, Proc. of the LANE'94, Vol. 1, pp. 361-370

Vollertsen, F., 1994, "Mechanism and models for laser forming," Laser Assisted Net Shape Engineering, Proc. of the LANE'94, Vol. 1, pp. 345-360